International Journal for Interdisciplinary Scientific Advancements (*IJISA*)
ISSN: 3085-5012

IJISA, 202,6 Volume 7, Issue 1, Page 16-31

Combined Stoichiometric and Theoretical Investigation of the Alkylation of 5-Nitro-1H-benzo[d]imidazol-2(3H)-one

Rachida Amanarne[a*], Mohamed Bougdem[a], Younes Ouzidan[a]

[a] *Laboratory of Physical Chemistry and Biotechnologies of Biomolecules and Materials, Faculty of Sciences and Technic Mohammedia, Hassan II University of Casablanca, Mohammedia, Morocco*

[b] *Higher Institute of Nursing Professions and Health Techniques (ISPITS) in Oujda, Oujda 60000, Morocco*

**Corresponding Author: rachidaamanarne@gmail.com (R. Amanarne)*

Received: 01/02/2026
Revised: 23/02/2026
Accepted: 18/03/2026
Published: 19/03/2026

Abstract:

In this paper, we report the synthesis of new heterocycl containing the benzimidazole nucleus. Imidazol nitrogen was alkyled using potassium carbonat as the base with the presence of a catalytic quantity of tetra-n-butylammonium bromide under mild condition. The structures of these products were determined using ^{1}H NMR, ^{13}C NMR and MS, the crystalline structure of some compounds obtained from X-ray diffraction confirms our proposed structures Along with the experimental data, the predicted spectral data were also obtained using density functional theory (DFT) at the B3LYP/6-31G basis set. In addition, the closest contacts between the active atoms of the compounds were identified through Hirshfeld surface analysis. Electrostatic potential maps were analyzed to predict functional group reactivity. Frontier Molecular Orbital (FMO) analysis revealed varying stability levels among the compounds, with 3b and 3c exhibiting slightly higher stability. Chemical potential and hardness analyses highlighted that these parameters suggest the electronic properties of the studied compounds may promote favorable interactions with biological targets, indicating their potential as promising therapeutic candidates among the investigated compounds.

Keywords: Benzimidazole, X-ray, alkylation, DFT.

Introduction

Nitrogen containing heterocyclic compounds includes a large number of physiologically active substances (Ferguson & Denny, 1995) (Yan et al., 2025). Moreover, they are valuable synthones for a wide variety of practically useful chemicals. In particular, Benzimidazoles are very useful intermediates/subunits for the development of molecules with pharmaceutical or biological interest. Benzimidazole derivatives have a wide range of biological activities, such as anti-diabetic (Wang et al., 2023), anti-antiproliferative (Gryshchenko et al., 2016), anti-fungals (Poyraz et al., 2008) and anti-Anti-inflammatory (Prajapat & Talesara, 2016).

As a continuation of our research work devoted to the development of substituted benzimidazol-2-one derivatives (Ouzidan et al., n.d.), we report in this paper the synthesis of new benzimidazol-2-one derivatives by action of the various carbon chains bromide on 5-nitro-1,3-dihydro-benzimidazol-2-one. We have obtained both derivatives di-and mono-substituted.

To gain deeper insight into the structural organization of the synthesized compounds, Hirshfeld surface (HS) analysis was employed to examine the intermolecular interactions and crystal packing features. This approach enables both qualitative visualization and quantitative assessment of non-covalent interactions, facilitating the identification of key contacts such as O–H···O, N–H···O, N–H···N, and C–H···O interactions that play a crucial role in stabilizing the crystal architecture (Öztürk et al., 2025).

In parallel, computational studies based on Density Functional Theory (DFT) were carried out to elucidate the electronic structure and global reactivity descriptors of compounds 3a–3c. These theoretical methods provide valuable information regarding charge distribution, frontier molecular orbitals, and intrinsic reactivity parameters. Furthermore, electrostatic surface potential (ESP) mapping was conducted to visualize electron density distribution and to identify potential reactive sites that may govern intermolecular interactions and chemical behavior (Zeng et al., 2025).

The combination of experimental synthesis, crystallographic analysis, and theoretical modeling offers a comprehensive framework for understanding the structure–reactivity relationships of these benzimidazol-2-one derivatives, and for assessing the impact of structural modifications on their electronic properties and potential biological relevance.

Results and discussion

Initially we have synthesized the 5-nitro benzimidazolone **1** by adopting the method of condensation

of 4-nitrobenzene-1,2-diamine and ethylechloroformate ('ChemInform Abstract', n.d.).

The N-alkylation reactions of benzimidazoles are an important research topic in the development of new heterocyclic derivatives of benzimidazole-based. In the same context, and in order to obtain new mono- and di-substituted benzimidazole derivatives, we examined the action of various brominated carbon chains on benzimidazolone **1**.

For this reason, we reacted compound **1** with bromo alkane chains (n = 8, 9, 10) in DMF using potassium bicarbonate as a base under the conditions of phase transfer catalysis (PTC).

The selected catalyst is tetrabutyl ammonium bromide (TBAB). In a first test, we reacted 5-nitro-1H-benzo [d] imidazol-2 (3H)-one with 2 equivalents of alkylating agent. In this case, only the dialkylated products are obtained. By decreasing the stoichiometric amounts of the alkylating agent, we obtained both mono and dialkyl derivatives; we also note a decrease in yield of dialkylated products for the benefit of mono alkylated products.

Duo to the lack of symmetry in the molecule **1**, the alkylation reactions led to the formation of two types of mono alkylated products. One obtained by the alkylation of nitrogen benzimidazolic in position 1; and the other one by the alkylation of nitrogen benzimidazolic in position 3. (scheme 1).

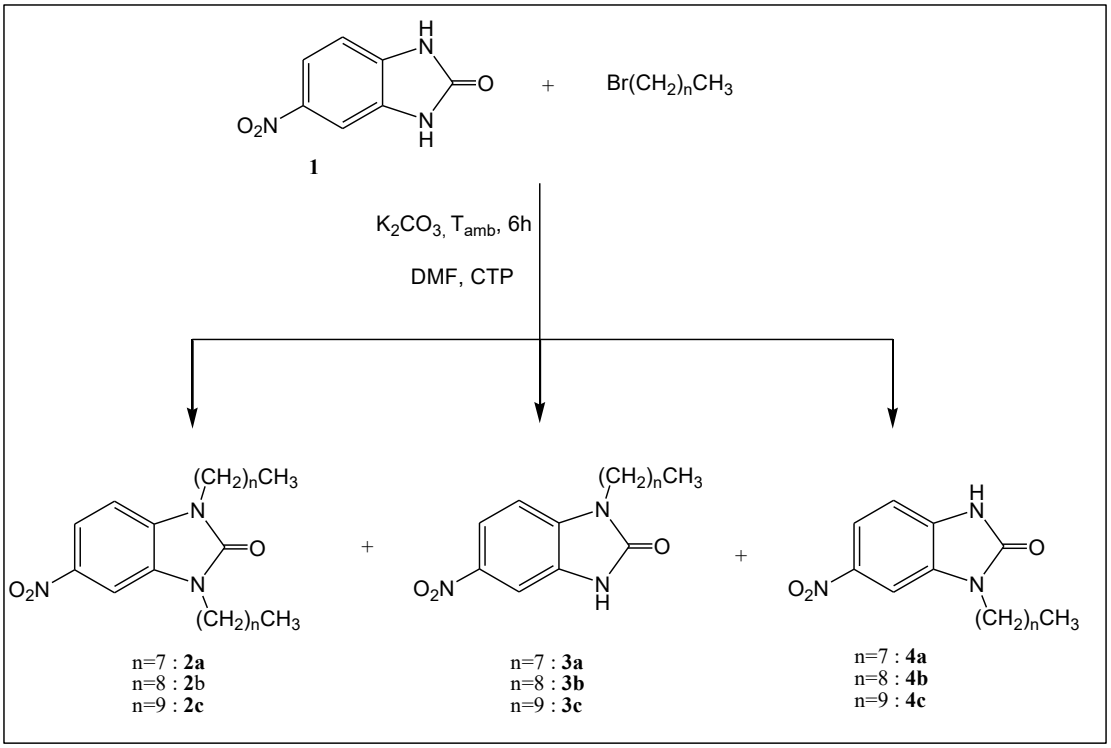

Scheme 1: Synthesis of 5-nitro benzimidazolone derivatives.

The table 1 below shows the synthesized products and their yields in different stoichiometric amounts.

Table.1. Yield of products **2-4(a-c)** in different reaction conditions.

Equivaler	n= 7	Yield	n=8	Yield	n=9	Yield
2 eq	**2a**	85	**3a**	87	**4a**	87
1.5 eq	**2a**	52	**3a**	54	**4a**	57
	2b	15	**3b**	16	**4b**	18
	2c	3	**3c**	3	**4c**	4
1.2 eq	**2a**	28	**3a**	28	**4a**	31
	2b	23	***3b***	25	**4b**	24
	2c	12	**3c**	12	**4c**	8
1 eq	**2a**	14	**3a**	13	**4a**	17
	2b	27	**3b**	27	**4b**	28
	2c	13	**3c**	12	**4c**	10

The crystallographic study of the products 3a, 3b and 3c allowed us to distinguish unambiguously between the three pairs of regioisomers (2a, 3a), (2b, 3b) and (2c, 3c).

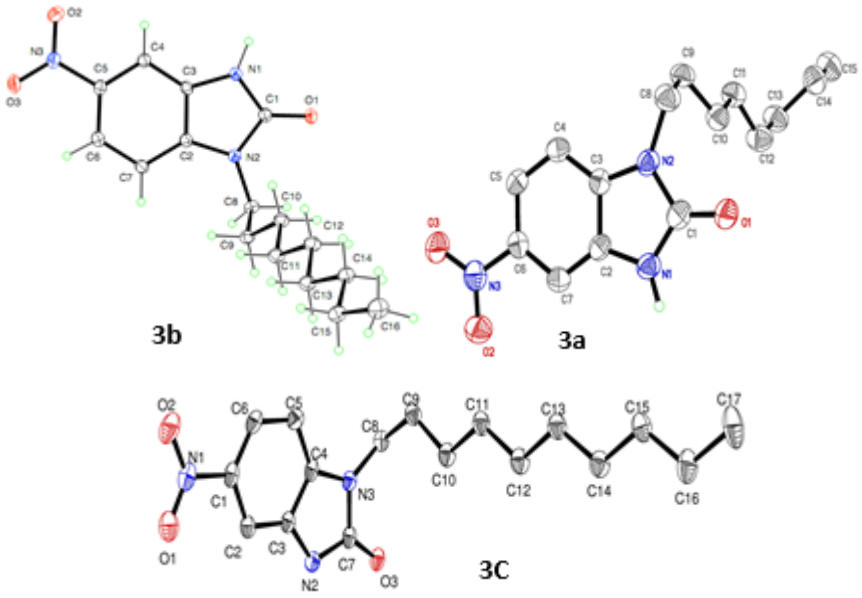

Fig. 1. ORTEP plots for the X-ray structures of compounds **3a-c**,the thermal ellipsoids are drawn at the 50% probability level.

Computational study

Hirshfeld surface analysis

Hirshfeld surface analyses of compounds (3a–c) were performed using the *Crystal Explorer 21.5* program (Spackman et al., 2021). The Hirshfeld surface (HS) approach was employed to investigate the intermolecular interactions and packing features of the studied crystal structures. This method enables a detailed visualization and quantitative evaluation of non-covalent interactions, particularly O–H···O, N–H···O, N–H···N, and C–H···O hydrogen bonds, which play a crucial role in the stabilization of the crystal lattice (Aqib et al., 2025).

The HS were mapped using the normalized contact distance (d_{norm}) within the range of −0.5 to 1.5 Å, enabling a three-dimensional representation of close intermolecular contacts. On the d_{norm} surfaces, red regions denote contacts shorter than the sum of the van der Waals radii, white regions correspond to contacts approximating van der Waals separations, and blue regions indicate longer intermolecular distances (Lanez et al., 2025). As illustrated in Fig. 2, distinct red spots and circular depressions are evident on the Hirshfeld surfaces of compounds 3a–3c, confirming the presence of significant short-range interactions.

These features are mainly associated with strong hydrogen-bonding interactions that govern the crystal packing and significantly enhance structural stability. Variations in the size, intensity, and distribution of the red regions among compounds 3a, 3b, and 3c reveal differences in intermolecular interaction strength and packing arrangements within the crystal lattice.

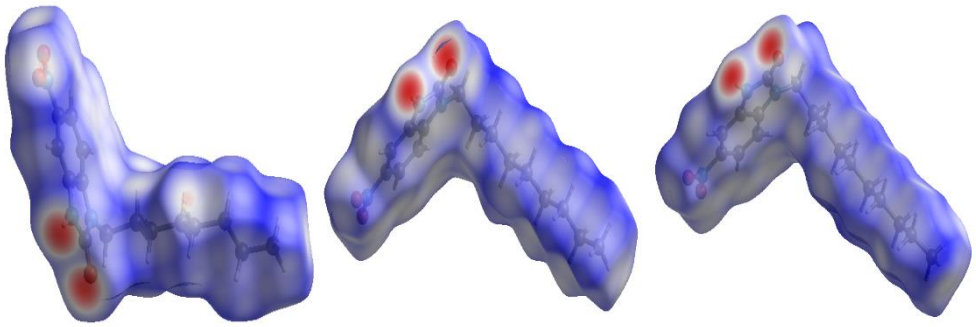

3a **3b** **3c**

Fig. 2. Hirshfeld surfaces of compounds (**3a–c**) mapped over the normalized contact distance (d_{norm}), showing the front view.

The two-dimensional (2D) fingerprint plots derived from the Hirshfeld surface analysis provide a quantitative and visual description of the intermolecular interactions contributing to the crystal packing of compound 3c. These plots represent the distribution of internal (d_i) and external (d_e) contact distances, allowing the identification and relative contribution of different atom–atom interactions to the Hirshfeld surface.

As shown in Fig. 3, the full fingerprint plot (100%) exhibits a characteristic asymmetric distribution, reflecting the anisotropic nature of intermolecular interactions in the crystal lattice. The dominant contribution arises from H···H interactions, accounting for 59.7% of the total Hirshfeld surface area, as indicated by the broad central region. This prevalence suggests that van der Waals interactions involving hydrogen atoms play a major role in stabilizing the crystal structure.

The O···H/H···O contacts, contributing 24.7%, appear as sharp, well-defined spikes at lower d_i and d_e values, which are characteristic of strong hydrogen-bonding interactions. These contacts indicate the presence of significant O–H···O hydrogen bonds that contribute to the cohesion and directional organization of the molecular assembly.

Minor contributions are observed for C···H/H···C interactions (5.9%), manifested as diffuse wing-like features, reflecting weak C–H···π or C–H···C contacts. Additionally, C···O/O···C interactions account for 3.2%, while N···H/H···N interactions contribute 2.1%, appearing as narrow lateral features and confirming the involvement of nitrogen atoms in weak hydrogen bonding.

Overall, the relative proportions and characteristic shapes of the fingerprint plots demonstrate that the crystal packing of compound 3c is governed primarily by H···H and O···H interactions, with additional contributions from weaker C···H, C···O, and N···H contacts. These interactions collectively lead to the formation of a stabilized three-dimensional supramolecular network within the crystal lattice.

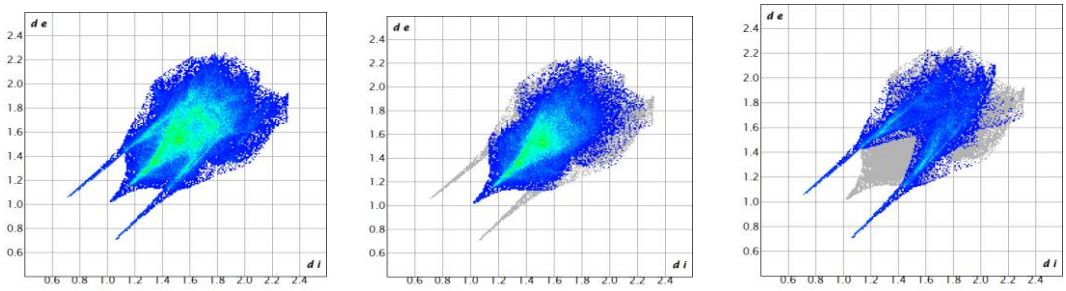

All (100%) H···H/H···H (59.7%) O···H/H···O (24.7%)

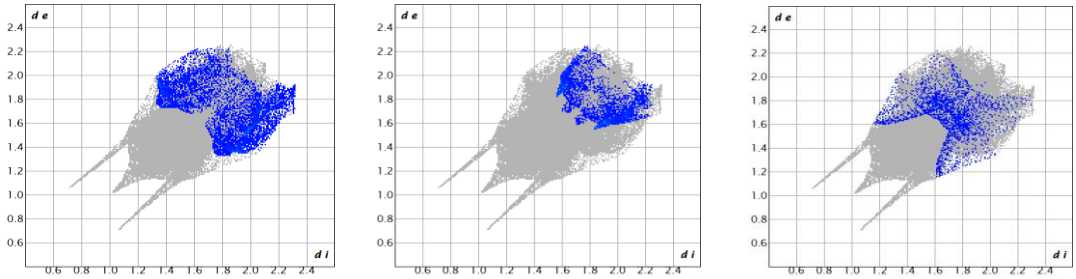

C···H/H···C (5.9%) C···O/O···C (3.2%) N···H/H···N (2.1%)

Fig. 3. The two-dimensional fingerprint plots of intermolecular interactions to the Hirshfeld surface area of compound **3c**.

DFT calculations

Reactivity study

5-nitro-1H-benzo [d] imidazol-2(3H)-one has two sites to be alkylated: the nitrogen at position 1 (N1) and the nitrogen at position 3 (N3). However, the reactivity of the nitrogen N1 is larger than that of nitrogen N3. In order to understand this difference in reactivity, we considered a theoretical study of the structure **1** by adopting the DFT methods with the B3LYP functiona (*Becke1988 B3LYP*, n.d.).

The basis is 6-31G. The analysis of results obtained using the Gaussian 09 program has allowed us to deduce the geometry optimized structure (Figure 4). System power results and atomic charges of nitrogen N1 and N3 are shown in the table below.

Table 2. Atomic charges and energy of compound 1

Energie		**tomic Charge**	
Ua	Kcal/mol	N1	N3
-659.4119195	-413780,979	**-0,783**	**-0,779**

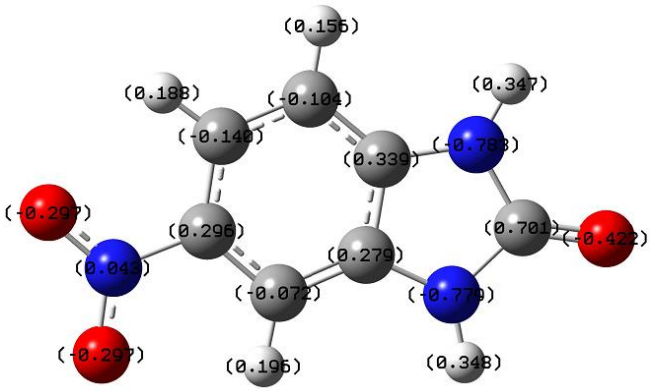

Fig. 4. optimized structure of compound **1**

It is shown above that the atomic charge in N1 nitrogen is higher than in N3 nitrogen.

Products investigations

Study of compound stability

To understand the stability of the different regioisomers obtained through alkylation of the benzimidazolone by alkyl bromides, we performed a calculation of the energies of each regioisomer. The table below shows the energies calculated for each compound.

Table.3. Calculated energies of the alkylated products at the N1 and N3 positions.

Length chain	Compound N_1 alkyled	Energy E_1 (Kcal/mol)	Compound N_3 alkyled	Energy E_3 (Kcal/mol)	E_3-E_1 (Kcal/mol)
n=8	**3a**	-611084,076	**4a**	-611083,96	**0,116**
n=9	**3b**	-635750,839	**4b**	-635750,681	**0,158**
n=10	**3c**	-660414,063	**4c**	-660413,946	**0 ,117**

From the table 3, we see that the energies of alkylated products on the N3 nitrogen have higher energies compared to those alkylated on nitrogen N1; therefore, the predominant formation of the alkylated compounds in N1 position is due to their energy stability.

Frontier molecular orbital (FMO):

Density Functional Theory (DFT) calculations were carried out to elucidate the electronic structure and reactivity features of compounds 3a, 3b and 3c. The spatial distribution of the frontier molecular orbitals (HOMO and LUMO), presented in Fig. 5, provides valuable insight into their

potential chemical behaviour. In all three molecules, the HOMO density is mainly localized over the heterocyclic core and the conjugated region, indicating that these fragments represent the primary electron-donating (nucleophilic) centres. Conversely, the LUMO orbitals are predominantly distributed over the terminal substituent and adjacent aromatic/alkyl moieties, suggesting that these parts of the molecules act as electron-accepting (electrophilic) regions during possible intermolecular interactions.

The energy gap (ΔE) is a crucial parameter for predicting molecular stability and reactivity, as smaller gaps generally correspond to higher electronic softness and enhanced reactivity, whereas larger gaps are associated with greater chemical stability (Rabee et al., 2025). Among the investigated compounds, 3a exhibits the lowest ΔE value (2.66 eV), indicating the highest electronic reactivity and potential capability to interact effectively with biological targets. In contrast, 3b (3.75 eV) and 3c (3.66 eV) display relatively larger band gaps, reflecting increased stability and reduced reactivity. These observations suggest that structural modifications significantly influence electron distribution and reactivity within this molecular series, and may therefore play a decisive role in determining their biological performance.

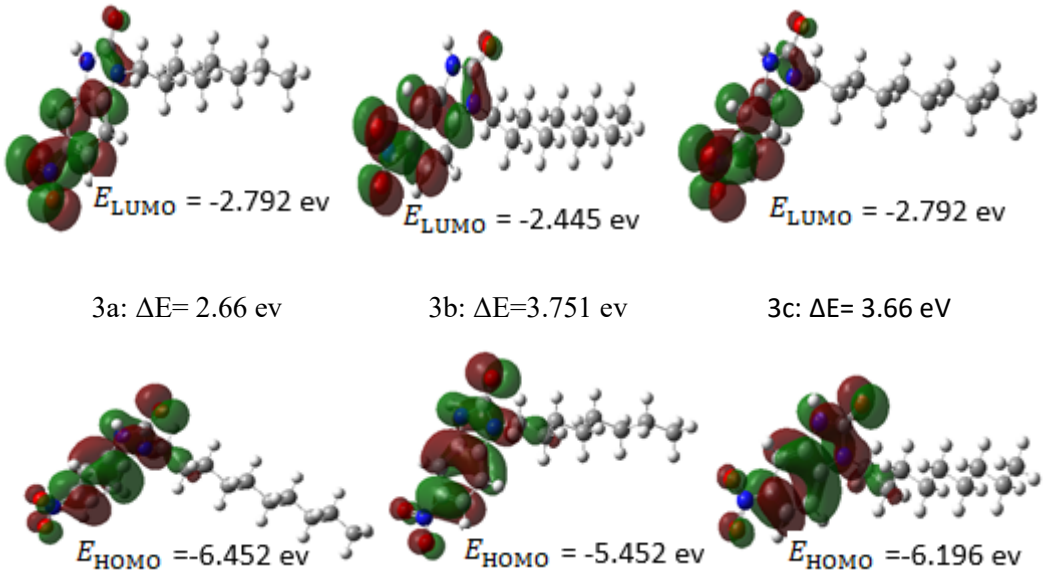

Fig.5. DFT calculated HOMO, LUMO, and energy gap for **3a**, **3b**, and **3c** at the B3LYP/6–31 G level of theory.

Conceptual Density Functional Theory (CDFT)

Conceptual Density Functional Theory (CDFT) was applied to investigate the global reactivity descriptors of compounds 3a–3c at the B3LYP/6-31G level of theory. The electronic chemical

potentials (μ) decrease progressively from −4.122 eV (3a) to −4.622 eV (3c), indicating an increasing tendency to accept electron density and a gradual enhancement of electron-deficient character, with 3c acting as the strongest electron acceptor in the series. The chemical hardness (η) values (1.33 eV for 3a, 1.8755 eV for 3b, and 1.83 eV for 3c) reveal that 3a is the softest and most polarizable system, favoring charge-transfer interactions, whereas3b and 3c exhibit greater resistance to electronic deformation and thus higher intrinsic stability. Consistently, the softness (S) values follow the inverse trend of hardness. The electrophilicity index (ω = 4.98–6.39 eV) classifies all compounds as strong electrophiles (ω > 1.5 eV) (Mellaoui et al., 2024), with 3a displaying the highest electrophilic power, confirming its strong ability to stabilize additional electronic charge. In contrast, the nucleophilicity index (N) indicates that 3a (6.71 eV) behaves as a strong nucleophile, while 3b (3.31 eV) and 3c (3.05 eV) exhibit moderate nucleophilic character (table 4). Overall, these CDFT parameters suggest that the electronic properties of the studied compounds may promote favorable interactions with biological targets, indicating their potential as promising therapeutic candidates.

Table.4. B3LYP/6-31G EHOMO, ELUMO, Energy gap ΔE, chemical potential (μ), chemical hardness (η), electronegativity (χ), softness (S) and electrophilicity (ω) in eV, of three compounds 3a-3c.

Product	E_{HOMO}	E_{LUMO}	μ	χ	η	S	ω	N
3a	-5,452	-2,792	-4,122	4,122	1,33	0,665	6,38755038	6,7138135
3b	-6,196	-2,445	-4,3205	4,3205	1,8755	0,53319115	4,97646501	3,3098135
3c	-6.452	-2.792	-4.622	4.622	1.83	0.54644809	5.83685355	3.0538135

Electrostatic Surface Potential (ESP) maps

Electrostatic Surface Potential (ESP) maps were generated in order to visualize the charge distribution and identify the potential reactive sites of compounds 3a, 3b and 3c (Fig. 6). The ESP surfaces clearly reveal regions of negative electrostatic potential (red to yellow), typically associated with electron-rich domains capable of interacting with electrophilic species, and regions of positive electrostatic potential (blue), corresponding to electron-deficient areas that may preferentially attract nucleophilic reagents (Sert et al., 2020). For all three compounds, the most intense negative potential regions are mainly localized around the carbonyl oxygen and nearby heteroatoms, confirming their role as strong nucleophilic centres. Conversely, the positive potential zones are predominantly concentrated around protonated or electron-withdrawing substituents, especially near the nitrogen atoms of the heterocyclic framework, indicating their electrophilic character.

A comparative analysis of the three molecules demonstrates that compound 3a exhibits relatively broader regions of negative potential compared to 3b and 3c, suggesting a higher tendency to participate in electrophilic interactions. In contrast, 3b and 3c display more balanced potential distributions, which may correlate with enhanced electronic stabilization. The observed ESP patterns are consistent with the HOMO–LUMO findings, supporting the hypothesis that variations in charge distribution may significantly influence molecular reactivity, interaction with biological targets, and overall activity profile (Yan et al., 2025). These insights highlight the importance of electrostatic features in governing molecular recognition and potential binding affinity with biological macromolecules.

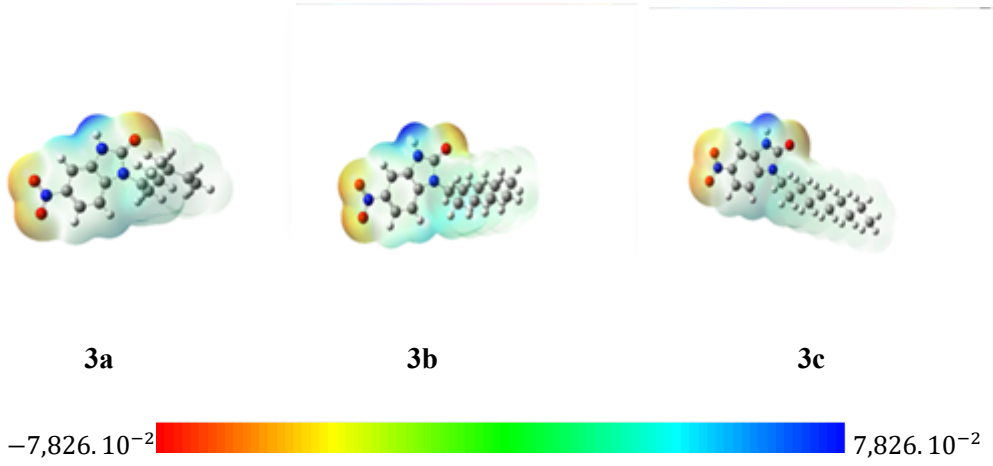

Fig. 6. Electrostatic surface potential maps for **3a**, **3b**, and **3c** at B3LYP/6–31 G level of theory.

Experimental section

^{13}C NMR spectra were recorded at 75 MHz, ^{1}H NMR spectra at 300 MHz. ^{1}H and ^{13}C chemical shifts (δ) are given in ppm relative to TMS as internal standard. Multiplicities are expressed as follows: singlet = s, doublet = d, and multiplet = m. Melting points were taken with a KOFLER hot stage apparatus and are uncorrected.

General procedure

To a solution of 5-nitro-1H-benzo[d]imidazol-2(3H)-one (0.2 g, 1.1 mmol), potassium carbonate (0.30 g, 2.2 mmol) and tetra-n-butylammonium Bromide (0.07 g, 0.2 mmol) in DMF (15 ml) was added 2.2, 1.65, 1.32 et 1.1 mmole of alkilating agent, Stirring was continued at room temperature for 6 hours. The salts were removed by filtration and the filtrate concentrated under reduced pressure. The residue was separated by chromatography on a column of silica gel with ethyl acetate/hexane (1/2) as eluent.

Conclusions

In this work, optimized reaction conditions were successfully developed for the synthesis of new mono- and di-substituted benzimidazol-2-one derivatives at positions 1 and 3 via N-alkylation using potassium carbonate as a base and TBAB as a phase-transfer catalyst. Hirshfeld surface analysis demonstrated that the crystal packing is predominantly governed by H···H and O···H interactions, which contribute significantly to the stabilization of the supramolecular structure.

DFT and CDFT calculations revealed that structural modifications strongly influence electronic distribution and molecular reactivity. Compound 3a exhibited the highest softness and electronic reactivity, whereas 3b and 3c showed comparatively greater stability. Electrostatic surface potential (ESP) analysis identified the carbonyl oxygen as the principal nucleophilic site, consistent with frontier molecular orbital findings.

Overall, the combined structural and theoretical results suggest that these compounds possess favorable electronic and reactivity profiles, indicating their potential as promising candidates for further investigation as therapeutic targets.

Compound 2a: 5-nitro-1,3-dioctyl-1H-benzo[d]imidazol-2(3H)-one:

mp(°C) = 44, RMN ^{1}H ($CDCl_3$, 300 MHz) δppm : 8.09(dd, 1H, H_{Ar}, J_1= 8.7Hz, J_2 = 2.1Hz) ; 7.88(d, 1H, H_{Ar}, J=2.1 Hz) ; 7.03 (d,1H, H_{Ar}, J=8.7Hz) ; 3.9-3.94(m, 4H, CH_2) ; 1.73-1.77(m, 4H, CH_2) ; 1.2-1.42(m, 20H, CH_2) ; 0.86(t, 3H, CH_3, J=6Hz). RMN ^{13}C ($CDCl_3$, 75MHz) δppm : 154.79(C=O) ;142.70, 135.04, 129.76(Cq) ; ; 118.53, 107.02, 103.73 (CH_{Ar}) ; 42.02, 41.98 (CH_2,N-CH_2) ; 32.12, 29.54, 28.72, 28.67, 27.14, 22.98(CH_2) ; 14.45 (CH_3).

Compound 2b : 5-nitro-1-octyl-1H-benzo[d]imidazol-2(3H)-one :

mp(°C) =134. RMN ^{1}H ($CDCl_3$, 300 MHz) δppm : 10.6,(s,1H,NH) ; 8.06-8.14(m, 1H,H_{Ar}) ; 7.08(d, 2H, H_{Ar}, J=8.4 Hz) ; 3.93 (t, 2H, CH_2, J = 6.6Hz) ;1.78-1.83(m, 2H, CH_2) ; 1.27-1.4(m, 10 H, CH) ; 0.88(t, 3H, CH_3, J=7.2Hz). RMN ^{13}C ($CDCl_3$, 75 MHz) δppm : 155.48 (C=O)143.08,135.79,128.17(Cq) ; 118.85, 107.54, 106.01(CH_{Ar});41.91(CH2,N-CH_2) ; 32.13 ; 29.57, 29.53, 28.77, 27.21, 22.99(CH_2); 14.46(CH_3).

Compound 2c : 6-nitro-1-octyl-1H-benzo[d]imidazol-2(3H)-one

mp(°C) = 134. RMN ^{1}H ($CDCl_3$, 300 MHz) δppm : 9.99 (s,1H,NH) ; 8.09 (dd,1H,H_{Ar}, J_1=8.7 Hz, J_2=2.1Hz) ;7.9 (d, 1H, H_{Ar}, J = 2.1Hz) ;7.17(d, 1H, H_{Ar}, J=8.7 Hz) ; 3.93 (t, 2H, CH_2, J = 7.5Hz) ; 1.76-1.85(m, 2H, CH_2) ; 1.25-1.39(m,10H, CH) ;0.87(t, 3H,CH_3). RMN ^{13}C ($CDCl_3$, 75 MHz) δppm : 155.34 (C=O) ; 142.45, 133.04, 130.4 (Cq) ; 118.57 ; 108.16 ; 105.69(C,CH_{Ar}) 41.747, 31.92, 29.72, 29.69, 29.57, 29.51, 29.35, 29.23, 28.31, 26.81, 22.70(CH_2) ;14.31(CH_3).

Compound 3a : 5-nitro-1,3-dinonyl-1H-benzo[d]imidazol-2(3H)-one

mp (°C) = 52. RMN^{1}H (DMSO-d_6, 300 MHz) δ ppm : 8.07(dd, 1H, H_{Ar}, J_1=8.7Hz, J_2=2.1 Hz) ; 7.86 (d, 1H, H_{Ar}, J=2.1 Hz) ; 7.01(d, 1H, H_{Ar}, J=8.7 Hz) ; 3.88-3.91(m, 4H, N-CH_2-) ; 1.74 - 1.76(m, 4H, 2 CH_2) ; 1.24-1.33 (m, 24H, 12 CH_2) ; 0.85 (m, 6H, 2 CH_3). RMN ^{13}C (DMSO) δppm : 154.42(C=O) ; 142.35, 134.68, 129.4(Cq) ; 118.16 , 106.97, 103.36(C, CH_{Ar}) ; 41.66, 41.62, 31.82, 29.44, 29.43, 29.21, 28.34, 28.30, 26.77, 22.65 (CH_2) ; 14.09, (CH_3).

Compound 3b: 5-nitro-1-nonyl-1H-benzo[d]imidazol-2(3H)-one

mp(°C) = 120°C. RMN^{1}H (DMSO-d_6, 300 MHz) δ ppm : 9.81(s, 1H, NH) ; 8.02-8.05(dd, 1H, H_{Ar}, J_1=8.7 Hz, J_2=2.1Hz) ; 7.85 (d, 1H, H_{Ar}, J=2.1 Hz) ; 7.12(d, 1H, H_{Ar}, J=8.7 Hz) ; 3.88(t, 2H, N-CH2, J= 7.5Hz) ; 1.20-1.80(m, 14H, 7 CH_2) ; 0.82(t, 3H, CH_3, J= 7.2 Hz). RMN ^{13}C (DMSO-d_6, 75 MHz) : 155.34(C=O) ; 142.45 ; 133.04 ; 130.41(Cq) ; 118.24, 108.51, 103.54 (CH_{Ar}) ; 41.47, 31.92, 29.72, 29.69, 29.62, 29.57, 29.35, 29.23, 28.31, 26.81, 22.70, (C, CH_2) ; 14.31 (C, CH_3).

Compound 3c : 6-nitro-1-nonyl-1H-benzo[d]imidazol-2(3H)-one

mp(°C) = 134. RMN^{1}H (DMSO-d_6, 300 MHz) δ ppm : 10.39(s, 1H, NH) ; 8.11(dd, 1H, H_{Ar}, J_1=8.7 Hz, J_2=2.1Hz) ; 8.05(d, 1H, H_{Ar}, J=2.1 Hz) ; 7.05(d, 1H, H_{Ar}, J=8.7Hz) ; 3.94(t, 2H, N-CH_2, J =7.2Hz) ; 1.84 (t, 3H, CH_3); 0.86-1.81 (m, 14H, 7 CH_2). RMN ^{13}C (DMSO-d_6, 75 MHz) : 156(C=O) ; 142.71, 135.44, 127.72 (Cq) ; 118.32 , 107.16, 106.66(CH_{Ar}) ; 41.54, 31.82, 29.44, 29.23, 29.21, 28.38, 26.83, 22.64 (CH_2) ; 14.10 (CH_3).

Compound 4a : 1,3-didecyl-5-nitro-1H-benzo[d]imidazol-2(3H)-one :

mp(°C) = 46. RMN ^{1}H (DMSO) δppm : 8.06(dd,1H,H_{Ar}, J_1=8.55Hz, J_2=2.1Hz) ; 7.85(d,1H,H_{Ar}, J=2Hz) ; 7(d,1H,H_{Ar}, J=5.7Hz) ; 3.9-3.65(m,4H,CH_2) ; 3.85-3.6(m,4H,CH_2) ; 1.55-1.15(m,14H,

CH_2) ; 0.83(m, 6H, CH_3). RMN ^{13}C (DMSO-d_6, 75 MHz) : δppm : 154.4(C=O) ; 142.3, 134.66, 129.36(Cq) ; 118.17, 106.65, 103.37(CH_{Ar}) ; 41.61, 31.88, 29.51, 29.28, 29.22, 28.33, 26.78, 22.88(CH_2) ; 14.14(CH_3).

Compound 4b : 1-decyl-5-nitro-1H-benzo[d]imidazol-2(3H)-one:

mp (°C) =98. RMN ^{1}H (DMSO-d_6, 300 MHz) δ ppm :1H:10.58(s, 1H, NH) ;8.04(dd, 1H, H_{Ar}, J_1 = 8.7Hz, J_2=2.1Hz) ;7.98(d, 1H, H_{Ar}, J = 2.1Hz) ;6.99(d, 1H, H_{Ar},J=8.4Hz) ;3.9-3.85(m,2H, CH_2) ; 2.04(m, 2H, CH_2) ;1.29-1.17(m,14H,CH_2) ; 3.2(t,3H,CH_3, J =7Hz). RMN ^{13}C (DMSO-d_6, 75 MHz) δppm :156.08(C=O) ;142.66,135.39, 127.78 (Cq), 118.46 , 107.18, 105.65(CH_{Ar}) ; 41.52, 31.85, 29.49, 29.27, 29.24, 28.39, 26.83, 22.67, 20.91, 20.85 (CH_2) ; 14.12(CH_3).

Compound 4c : 1-decyl-6-nitro-1H-benzo[d]imidazol-2(3H)-one :

mp (°C) =98. RMN^{1}H (DMSO-d_6, 300 MHz) δ ppm : 9.99(s, 1H, NH) ; 8.09(dd, 1H, H_{Ar}, J_1=8.7Hz, J_2=2.1Hz) ; 7.9(d, 1H, H_{Ar}, J=2.1 Hz) ; 7.17(d, 1H, H_{Ar}, J=8.7 Hz) ; 3.93(t, 3H, CH_3, J= 7.2Hz) ; 1.7-1.77(m, 2H, CH_2) ; 1.2-1.33(m, 14H, CH_2) ; 0.81(t, 3H, CH_3, J= 6.9Hz). RMN ^{13}C (DMSO-d_6, 75 MHz):155.34(C=O) ; 142.45; 133.04; 130.41(Cq) ; 118.46, 107.18, 105.65 (CH_{Ar}) ; 41.47; 31.92; 29.72 ; 29.69 ; 29.57 ; 29.35 ; 29.23 ; 28.31 ; 26.81 ; 22.70 (CH_2) ; 14.31(CH_3).

References

Ferguson, L. R., & Denny, W. A. (1995). Microbial mutagenic effects of the DNA minor groove binder pibenzimol (Hoechst 33258) and a series of mustard analogues. *Mutation Research - Fundamental and Molecular Mechanisms of Mutagenesis*, *329*(1), 19-27. https://doi.org/10.1016/0027-5107(95)00013-9

Yan, G., Wang, X., Wang, Y., Wei, L., Huang, Z., Yang, Z., Li, C., Zhou, Z., & Zheng, Z. (2025). Synthesis, crystal structure, DFT, vibrational properties, Hirshfeld surface and in vitro anti-proliferation studies of a novel sulfonamide-containing pyrazolo[1,5-a]pyridine derivative. *Journal of Molecular Structure*, *1346*, 143255. https://doi.org/10.1016/j.molstruc.2025.143255

Wang, X., Du, J., Zhou, T., Fang, X., & Yang, H. (2023). Novel benzotriazole-benzimidazole metal complexes : Structure-activity relationship, synthesis, characterization, and antidiabetic activity. *Journal of Molecular Structure*, *1292*, 136141. https://doi.org/10.1016/j.molstruc.2023.136141

Gryshchenko, A. A., Tarnavskiy, S. S., Levchenko, K. V., Bdzhola, V. G., Volynets, G. P., Golub, A. G., Ruban, T. P., Vygranenko, K. V., Lukash, L. L., & Yarmoluk, S. M. (2016). Design, synthesis and biological evaluation of 5-amino-4-(1H-benzoimidazol-2-yl)-phenyl-1,2-dihydro-pyrrol-3-ones as inhibitors of protein kinase FGFR1. *Bioorganic & Medicinal Chemistry*, *24*(9), 2053-2059. https://doi.org/10.1016/j.bmc.2016.03.036

Poyraz, M., Sari, M., Demirci, F., Kosar, M., Demirayak, S., & Büyükgüngör, O. (2008). Synthesis, crystal structure and biological activity of 1-(1H-benzoimidazol-2-yl)-ethanone thiosemicarbazone and its cobalt complex. *Polyhedron*, *27*(9-10), 2091-2096. https://doi.org/10.1016/j.poly.2008.03.030

Prajapat, P., & Talesara, G. L. (2016). Synthesis and Anti-inflammatory Screening of Some Mono and Bis-Alkoxyphthalimide Linked Benzimidazole and their Quinazoline and Pyrimidine Derivatives. *Journal of Heterocyclic Chemistry*, *53*(5), 1603-1610. https://doi.org/10.1002/jhet.2471

Ouzidan, Y., Rodi, Y. K., Misbahi, K., Chahdi, F. O., Ramchoun, M., & Essassi, E. M. (s. d.). *ETUDE STŒCHIOMETRIQUE DE LA REACTION D'ALKYLATION DE LA 5-NITRO-1H-BENZO[d]IMIDAZOL-2(3H)- ONE, VERS DES PRODUITS MONOALKYLES*.

Öztürk, K., Özkan, E. N., Çalışkan, Ç. E., Aytaç, S., & Aytaç, Ö. G. (2025). Synthesis, single crystal XRD, DFT, molecular docking studies and antioxidant capacity and antibacterial evaluation

of β -phenylethylamine derivative schiff base compound. *Journal of Molecular Structure*, *1344*, 143011. https://doi.org/10.1016/j.molstruc.2025.143011

Zeng, W., Yue, D., Wang, X., & Kong, X. (2025). Vibrational spectroscopy, DFT calculations, MEP, NBO, NLO and Hirshfeld surface studies of a new Meldrum's acid derivative containing 2-hydroxyphenylamino moiety. *Journal of Molecular Structure*, *1341*, 142675. https://doi.org/10.1016/j.molstruc.2025.142675

ChemInform Abstract : Synthesis of Benzimidazolone Derivatives Based on 2-Acylcyclohexane-1,3-diones Alkoximes. | Request PDF. (s. d.). *ResearchGate*. https://doi.org/10.1134/S1070428008070130

Spackman, P. R., Turner, M. J., McKinnon, J. J., Wolff, S. K., Grimwood, D. J., Jayatilaka, D., & Spackman, M. A. (2021). *CrystalExplorer*: A program for Hirshfeld surface analysis, visualization and quantitative analysis of molecular crystals. *Journal of Applied Crystallography*, *54*(3), 1006–1011. https://doi.org/10.1107/S1600576721002910

Aqib, M., Siddique, A., Atta, S., Javed, R., Qasim, M. N., AlDamen, M. A., Ahmad, A., Alshammari, A. Q., Alshammari, A. Q., Ibragimov, A. B., & Akhtar, M. N. (2025). Cu(II)-based complex with carboxylate moiety: Structure, characterization, Hirshfeld surface analysis and adsorption properties towards methylene blue. *Journal of Molecular Structure*, *1345*, 143074. https://doi.org/10.1016/j.molstruc.2025.143074

Lanez, T., Lanez, E., & Henni, M. (2025). Synthesis, crystal structure, Hirshfeld surface analysis, DFT studies and DNA binding interactions of N-ferrocenylmethyl-N-(3-cyanophenyl)acetamide. *Journal of Organometallic Chemistry*, *1038*, 123772. https://doi.org/10.1016/j.jorganchem.2025.123772

Becke1988 B3LYP. (n.d.).

Rabee, A. R., Hagar, M., Soliman, S. M., Abdel-Hamid, H., Jaremko, M., Emwas, A.-H., Elwakil, B. H., Hassan, A., & Bekhit, M. G. (2025). Design and synthesis of new 1,2,3-triazole/benzimidazole hybrids using Click reaction: Antibacterial evaluation, molecular docking, and DFT analysis. *Journal of Molecular Structure*, *1345*, 143066. https://doi.org/10.1016/j.molstruc.2025.143066

Mellaoui, M. D., Zaki, K., Abbiche, K., Imjjad, A., Boutiddar, R., Sbai, A., Jmiai, A., Issami, S. E., Lamsabhi, A. M., & Zejli, H. (2024). In silico anticancer activity of isoxazolidine and isoxazolines derivatives: DFT study, ADMET prediction, and molecular docking. *Journal of Molecular Structure*, *1308*, 138330. https://doi.org/10.1016/j.molstruc.2024.138330

Sert, Y., Lahmidi, S., El Hafi, M., Gökce, H., Essassi, E. M., Ejjoumamany, A., & Mague, J. T. (2020). Spectral, DFT/B3LYP and molecular docking analyses on ethyl 2-(5-methyl-1,2,4-triazolo[1,5-a]pyrimidin-7-yl)pent-4-enoate. *Journal of Molecular Structure*, *1206*, 127680. https://doi.org/10.1016/j.molstruc.2020.127680

Yan, G., Wang, X., Wang, Y., Wei, L., Huang, Z., Yang, Z., Li, C., Zhou, Z., & Zheng, Z. (2025). Synthesis, crystal structure, DFT, vibrational properties, Hirshfeld surface and in vitro anti-proliferation studies of a novel sulfonamide-containing pyrazolo[1,5-a]pyridine derivative. *Journal of Molecular Structure*, *1346*, 143255. https://doi.org/10.1016/j.molstruc.2025.143255